Chapter* Earth, Moon & Planets 80, 311-341

Preparing for the 1998/99 Leonid Storms

P. Jenniskens (1), M. de Lignie (2), H. Betlem (2), J. Borovicka (3),
C.O. Laux (4), D. Packan (4), C.H. Kruger (4)

1) NASA/Ames Research Center, Mail Stop 239-4, Moffett Field, CA 94035-1000 (peter@max.arc.nasa.gov); 2) Dutch Meteor Society, Lederkarper 4, 2318 NB Leiden, the Netherlands (betlem@strw.LeidenUniv.nl); 3) Astronomical Institute, 251 65 Ondrejov, Czech Republic (borovic@asu.cas.cz); 4) High Temperature Gasdynamics Laboratory, Bldg. 250, Mechanical Engineering Department, Stanford University, Stanford CA 94305-3032 (laux@saha.stanford.edu)

Key words: meteoroids - comets - atmosphere, dynamics - organic chemistry

Abstract: In order to further observing programs aimed at the possible meteor storms of November 1998 and 1999, we describe here how the Leonid shower is expected to manifest itself on the sky. We discuss: 1) the expected wavelength dependence of meteor (train) emission, 2) the meteor brightness distribution and influx, 3) the stream cross section, radiant and altitude of the meteors, 4) the apparent fluxes at various positions in the sky as a function of radiant elevation as well as 5) the trail length and radial velocity, and 6) the diameter and brightness of persistent trains as a function of radiant elevation. These topics were chosen to help researchers plan an observing strategy for imaging, spectroscopy, and LIDAR observations. Some applications are discussed.

1. Introduction

On November 17th, 1998, and again in 1999, the sky over eastern Asia (1998) and Europe (1999) will be in flames if the Earth, once more, will cross the fresh ejecta

*) Contributed chapter in: LABORATORY ASTROPHYSICS AND SPACE RESEARCH, P. Ehrenfreund, H. Kochan (eds.), Kluwer Acad. Publishers (1998, in press)

of comet 55P/Tempel-Tuttle that was mapped out by historic accounts of Leonid meteor storms (Yeomans 1981). Expectations are that meteor rates may increase above 1 per second for a period of an hour or more around the time of nodal passage. A once-in-a-lifetime opportunity for the study of cometary debris for its composition and dynamics, the interaction of meteoroids with Earth's atmosphere, and the upper atmosphere's chemistry and dynamics.

Historic accounts of Leonid storms date back to 902 AD. During each return of the comet, every 33 odd years, the encounter conditions with Earth's orbit are slightly different due to planetary perturbations of the comet orbit. The comet passed perihelion again on February 28, 1998. The present return mimics encounter conditions in 1866 and 1867, when rates increased to above 10,000 meteors per hour for a short period of time. On the other hand, conditions also do not differ too much from those during the 1932 return, when no meteor storm was reported (i.e. volleys of rates larger than 1/s).

The expected meteor rates based on meteor stream models (Wu and Williams 1996) and past observations of Leonid activity (Jenniskens 1996, Brown et al. 1997) have been discussed elsewhere as well as the orbital dynamics of comet 55P/ Tempel-Tuttle (Yeomans et al. 1996). In summary, both in November 1998 and in 1999 there is a chance that a Leonid meteor storm will occur with peak rates up to 2,000 - 10,000 meteors per hour visible for a single visual observer under a clear dark sky.

During a storm, Earth crosses the outer regimes of the dust trail of comet P/Tempel-Tuttle. The high flux allows unprecedented precision in characterizing the dust trail in terms of spatial and particle size distributions of dust grains and allows the measurement of composition, morphology and orbits of individual cometary grains relatively soon after ejection from the comet.

When the meteoric matter accretes into the Earth's atmosphere, new molecules and solid particles are formed that are of interest to the origin of life, the interaction of Earth and Space, and the issue of ozone depletion.

Leonid storm meteors are also unique probes of the upper atmosphere, notably the mesopause and lower ionosphere. Bright Leonids are first observed at 160 km altitude and penetrate to about 85 km altitude. Most mass is deposited at altitudes of 98-102 km, higher than matter from normal sporadic meteors. The parcel of atmosphere affected by the meteors can be analyzed by lidar, radar, and various other techniques to reveal gravity wave wind patterns in three dimensions, air turbulent motions, metal atom chemistry, etc.

The Leonid showers will be studied from an airborne observatory in a Leonid Multi-Instrument Aircraft Campaign, which will be a flying laboratory for flash-heating experiments on cosmic materials, high-velocity re-entry dynamics, and reaction chemistry experiments in the upper atmosphere. The techniques used in this mission will be mainly remote sensing imaging, spectroscopic, and ranging techniques. The present work came forth from preparatory work for this Leonid Multi-Instrument Aircraft Campaign.

Because of their unique character, the upcoming Leonid returns may be appealing also to researchers with little or no experience in meteor observing. For their benefit, we here provide basic information about how the Leonid shower is expected to manifest itself. We will concentrate on information that can help guide an observing strategy and is useful for determining the observing location and time period, the detection rate in a given part of the sky, the manifestation of the Leonid meteors on the detection devise (spectral output, trail length, angular velocity, train diameter), and the convergence angle for two-station imaging techniques for a range of meteor-station geometries.

We will mainly concentrate on optical detection techniques. Of course, other techniques exist. For example, the ionized train is an effective reflector of radio wavelengths, a technique used in radar observations of meteors. These will not be considered here because an extensive body of literature is available (e.g. McKinley 1961, McIntosh and Millman 1970).

2. Spectral Output

2.1. AT OPTICAL WAVELENGTHS

Meteors are studied by remote sensing. Here, we will concentrate on the expected optical and infrared output, wavelength regimes that are assessable from the ground. Meteors radiate strongly also in the ultra-violet and perhaps at soft X-rays. Meteors and trains are also expected to emit at submm wavelengths for which no information is available. On the other hand, radio emissions at very low frequencies have been detected.

The visual and near-infrared spectra of meteors in the range from 3500 Å to 9000 Å have been studied by photographic slit-less spectroscopic techniques. The spectra are dominated by electronic transitions of metal atoms and ions. The more intense transitions that originate in the ground state of the neutral species can be used for the measurement of neutral atom debris trails by LIDAR through resonant scattering (Kane and Gardner 1993).

The following 17 elements have been detected in meteor spectra: H, Li, C, Na, Mg, Al, Si, K, Ca, Ti, Cr, Mn, Fe, Ni, Cu, Sr, and Zr (Borovicka 1993; 1994). Most easily measured are the metallic ions Na, Mg, Si, Ca, Fe, and Ni. The excitation conditions and elemental abundances can be inferred from relative line strengths (Harvey 1973, Borovicka 1994). Typically, a “cold” (4000-5000 K) component is present, while a hot (10,000 K) component may be detected when a shock develops. A shock occurs when the particle is bigger than the mean free path of the atmospheric molecules. The cold component has given information on Fe, Ni, Cr, Ca, Mg, Si, Al, Mn, K, and Na, while the hot component also has given information on Ti and H, with some meteoric component of N and O.

In Table I are listed the expected relative intensities of atomic lines in the range 3500 - 7000 Å in Leonid meteor spectra. The intensities relate to the meteor head and the

sensitivity limit in the two models was set to correspond to that of good photographic records. One column gives the synthetic spectrum of a -10 magn. Leonid, including both the hot and cold spectral components. The other column is for a Leonid of lesser brightness (≥ +0 magn.), which has not develloped a shock. In intermediate cases, the high temperature component may be present but with lower intensity than listed here. Some close line pairs listed in the tables will not be resolvable in real spectra.

Meteor spectra can also contain emission bands of meteoric metal oxides (FeO, CaO, and AlO), hot air (N_2, O_2) and air fragments (N_2^+), as well as bands of C_2 and CN from the organic material in the meteoroids. The organic bands are expected to be prominent at early stages of meteor ablation, above 120 km altitude. The hot air bands are strongest in the 6300 - 6700 Å region and tend to blend with the CN bands at later stages in the meteoric process.

TABLE 1. Leonid spectrum in the near-UV/visual/near-IR. Columns list the line wavelength in air (Å), the expected relative line intensity for a -10 and a +0 Leonid respectively, and the line identification: the element, ionization degree and multiplet number. An asterix marks the spectral lines due to the hot component.

Wavelength	Intensity		Identification		Wavelength	Intensity		Identification	
(Å)	-10	+0 magn.			(Å)	-10	+0 magn.		
3513.82	2.5		Fe I	24	3905.53	1.5		Si I	3
3515.05	4.0	1.8	Ni I	19	3906.48	2.6		Fe I	4
3521.26	3.0	1.0	Fe I	24	3920.26	6.0	2.9	Fe I	4
3524.54	5.7	3.7	Ni I	18	3922.91	7.5	4.3	Fe I	4
3526.04	3.3	1.4	Fe I	-	3927.92	8.1	4.9	Fe I	4
3526.17	1.7		Fe I	24	3930.30	8.6	5.5	Fe I	4
3558.52	4.8	2.0	Fe I	24	3933.67	16.8	31.4	Ca II	1
3565.38	7.5	6.1	Fe I	24	3933.67	890.5		Ca II	1*
3570.10	8.7	10.8	Fe I	24	3961.53	2.2		Al I	1
3578.69	2.8	1.1	Cr I	4	3968.47	15.6	22.8	Ca II	1
3581.19	9.8	16.6	Fe I	23	3968.47	616.5		Ca II	1*
3585.32	4.2	1.5	Fe I	23	3969.26	5.1	1.6	Fe I	43
3585.71	2.4		Fe I	23	4005.24	3.4		Fe I	43
3586.98	4.0	1.4	Fe I	23	4030.76	4.9	2.2	Mn 1	2
3593.49	2.3		Cr I	4	4033.07	3.8	1.6	Mn I	2
3605.33	1.8		Cr I	4	4034.49	2.6	1.0	Mn I	2
3608.86	7.8	6.2	Fe I	23	4045.81	11.8	8.3	Fe I	43
3618.77	8.5	8.1	Fe I	23	4063.59	9.6	4.5	Fe I	43
3619.39	4.0	1.6	Ni I	35	4071.74	8.4	3.4	Fe I	43
3631.46	8.8	9.3	Fe I	23	4128.11	2.4		Si II	3*
3647.84	8.3	6.9	Fe I	23	4130.96	3.3		Si II	3*
3679.91	6.3	3.7	Fe I	5	4132.06	3.1		Fe I	43
3687.46	5.3	2.2	Fe I	21	4143.87	4.7	1.4	Fe I	43
3705.57	7.8	6.0	Fe I	5	4202.03	4.0	1.1	Fe I	42
3706.03	9.0		Ca II	3 *	4226.73	16.1	15.3	Ca I	2
3709.25	6.3	3.0	Fe I	21	4233.17	2.8		Fe II	27*
3719.93	12.0	23.8	Fe I	5	4250.79	3.6	1.0	Fe I	42
3722.56	8.0	6.1	Fe I	5	4254.35	2.3		Cr I	1
3727.62	6.3	2.9	Fe I	21	4260.47	2.9		Fe I	152
3733.32	7.3	4.8	Fe I	5	4271.76	10.0	4.3	Fe I	42
3734.86	11.6	19.1	Fe I	21	4274.80	1.8		Cr I	1

Wavelength (Å)	Intensity -10	+0 magn.	Identification		Wavelength (Å)	Intensity -10	+0 magn.	Identification	
3736.90	17.5		Ca II	3*	4289.72	1.3		Cr I	1
3737.13	11.5	20.4	Fe I	5	4294.12	1.9		Fe I	41
3743.36	5.0	1.9	Fe I	21	4300.05	1.6		Ti II	41*
3745.56	10.7	15.4	Fe I	5	4303.17	1.0		Fe II	27*
3745.90	7.7	5.3	Fe I	5	4307.90	10.4	4.6	Fe I	42
3748.26	9.5	10.0	Fe I	5	4325.76	10.9	4.9	Fe I	42
3748.49	1.2		Fe II	154*	4383.55	15.0	10.4	Fe I	41
3749.49	10.9	14.5	Fe I	21	4404.75	10.4	4.3	Fe I	41
3758.23	10.0	10.0	Fe I	21	4415.12	4.5	1.3	Fe I	41
3759.29	6.4		Ti II	13*	4481.24	38.4		Mg II	4*
3761.32	5.4		Ti II	13*	4549.47	1.2		Fe II	38*
3763.79	8.9	6.4	Fe I	21	4549.63	1.1		Ti II	82*
3767.19	7.9	4.5	Fe I	21	4558.66	1.0		Cr II	44
3787.88	4.7	1.7	Fe I	21	4583.83	2.4		Fe II	38*
3795.00	5.6	2.2	Fe I	21	4629.34	1.5		Fe II	37*
3798.51	3.7	1.2	Fe I	21	4861.33	1.4		H I	1*
3799.55	5.2	2.0	Fe I	21	4920.50	1.8		Fe I	318
3812.96	3.9	1.3	Fe I	22	4923.92	7.1		Fe II	42*
3815.84	9.1	5.6	Fe I	45	4957.60	2.7		Fe I	318
3820.43	11.9	16.8	Fe I	20	5018.43	11.0		Fe II	42*
3824.44	9.1	7.6	Fe I	4	5041.03	1.1		Si II	5*
3825.88	11.0	11.8	Fe I	20	5167.32	11.5	3.0	Mg I	2
3827.82	7.5	3.3	Fe I	45	5167.49	3.6	1.1	Fe I	37
3829.35	10.3	3.2	Mg I	3	5169.03	7.2		Fe II	42*
3832.30	14.1	6.9	Mg I	3	5172.68	23.8	8.6	Mg I	2
3834.22	9.4	6.8	Fe I	3	5183.60	29.6	13.7	Mg I	2
3838.29	16.5	12.0	Mg I	3	5227.19	2.5		Fe 1	37
3840.44	7.9	4.1	Fe I	20	5269.54	9.5	4.0	Fe I	15
3841.05	6.4	2.3	Fe I	45	5270.36	1.8		Fe I	37
3849.97	5.0	1.8	Fe I	20	5275.99	1.3		Fe II	49*
3853.66	1.0		Si II	1*	5316.61	1.8		Fe II	49*
3856.09	9.7		Si II	1*	5328.04	6.6	2.5	Fe I	15
3856.37	9.6	8.1	Fe I	4	5371.49	4.3	1.5	Fe I	15
3859.91	12.8	22.2	Fe I	4	5397.13	2.3		Fe I	15
3862.51	5.4		Si II	1*	5405.78	2.7		Fe I	15
3865.52	4.2	1.5	Fe I	20	5429.70	2.7		Fe I	15
3872.50	4.8	1.8	Fe I	20	5446.92	2.4		Fe I	15
3878.02	5.2	1.9	Fe I	20	5616.54	1.8		N I	24*
3878.57	8.9	6.4	Fe I	4	5889.95	40.7	40.7	Na I	1
3886.28	11.1	12.4	Fe I	4	5895.92	30.7	22.0	Na I	1
3887.05	3.9	1.3	Fe I	20	6158.19	1.0		O I	10*
3888.51	3.0		Fe I	45	6347.10	12.3		Si II	2*
3895.66	6.6	3.4	Fe I	4	6371.36	6.0		Si II	2*
3899.71	8.0	4.8	Fe I	4	6482.74	1.1		N I	21*
3902.95	3.9	1.1	Fe I	45	6562.82	6.7		H I	1*

2.2. AT INFRARED WAVELENGTHS

No spectroscopic information has been published on meteors or meteor trains in the near-infrared (1-3 micron), mid-infrared (3-20 micron) or far-infrared (20-200 micron). However, only 1 % of kinetic energy is emitted as near-UV and Visible luminosity (the “luminosity efficiency” for various detection techniques). A fraction of the remaining kinetic energy is expected to be lost by heating of the air in the meteoroid

path. The column of hot air is expected to cool by radiation escape (bound-bound, free-bound, and free-free transitions). In addition, dust from meteoric debris and recondensed vapor is expected to emit an emission continuum that may partially overlap the continuum of other sources.

In order to evaluate the expected infrared emission of meteor trains, emission spectra of shocked air have been calculated from thermal equilibrium models. The models are expected to approximate the emission from long lasting persistent trains after they have expanded to a state of pressure equilibrium with the surrounding air (1-2 minutes after a bright enough meteor has passed). For a fast Leonid, the temperature directly behind the shock was found to increase to close to a million K. The column of hot air will rapidly expand to pressure equilibrium with its surroundings, which will cool the air. Here we present the spectra of shocked air at relevant temperatures of 3000, 4500 and 6000 K. A pressure of P = 0.00991 Pa was assumed at 95 km altitude. A chemically active initial atmospheric composition of N_2: O_2: C: H with mole fraction 0.788:0.21:0.001:0.001 was assumed. At each temperature the equilibrium composition of the mixture at pressure P was computed using the NEQAIR2 code (Laux et al. 1995). The product molecular species incorporated in the calculations are all those important either by their mole fraction or by their emission intensity. The total number density is n = P/kT and mole fractions are listed in Table II. The model considered transitions of CN (Red), $N2^+$ (Meinel), NO (X-X, C-A, D-A, F-C, E-C, E-D, H-C, H-D, H'-C, H'-D), CO (X-X), and CO_2 (n_3). The resulting theoretical spectrum, parts of which are shown in Figures 1, was convolved by a triangular slit-function that reproduces the 0.0016 micron resolution of a Fabry-Perot spectrograph.

TABLE 2. Composition of shocked air in thermal equilibrium at 95 km

Component	Mole fraction*			Component	Mole fraction		
	3000 K	4500K	6000K		3000 K	4500K	6000K
e^-	2.2e-6	4.5e-4	4.9e-2	O_2	9.1e-6	3.5e-9	8.9e-11
CO	8.2e-4	1.4e-5	1.0e-9	C^+	6.7e-14	1.2e-4	4.3e-4
N^+	1.4e-12	1.8e-4	3.7e-2	H^+	8.9e-13	3.1e-7	3.2e-5
N_2	6.4e-1	7.3e-3	8.8e-6	NO	2.8e-4	2.0e-6	2.0e-8
OH	1.8e-8	1.6e-11	5.8e-13	O	3.4e-1	2.1e-1	1.9e-1
C	5.5e-9	3.7e-4	5.0e-5	CN	2.8e-10	4.8e-8	3.6e-11
H	8.2e-4	5.0e-4	4.4e-4	N	1.1e-2	7.8e-1	7.1e-1
NH	2.8e-11	1.0e-11	7.5e-13	NO^+	2.2e-6	3.2e-5	2.2e-6
N_2^+	1.4e-12	1.3e-7	8.0e-8	O^+	3.2e-10	1.1e-4	1.2e-2

*) total n 2.4e+18 / 1.61e+18 / 1.2e+18 m^{-3}

We find that the dominant emission at 3000 K is from the NO infrared transition (Fig. 1a). The CN Red band may also be detectable (Fig. 1b). Other bands are

neglegible. At 4500 K, the N_2^+ Meinel band dominates the spectrum (Fig. 1c), while the CN and N_2 bands are stronger and atomic lines of N and O are starting to

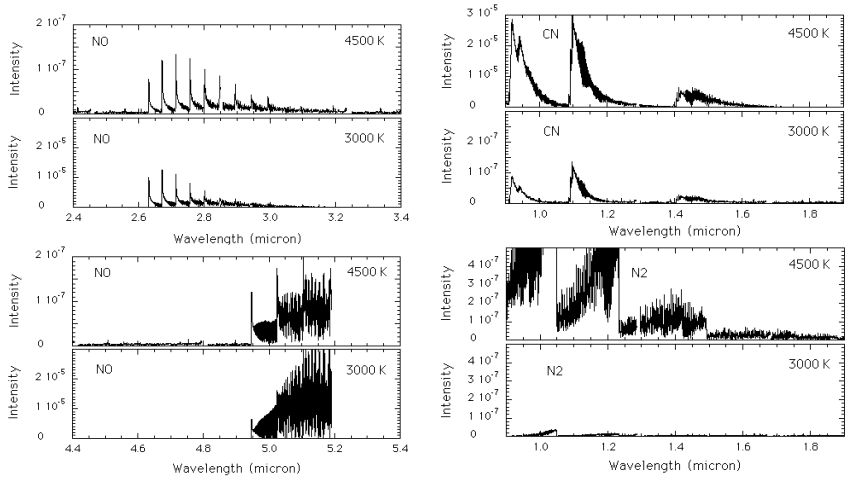

Figure 1 a (left). Theoretical near- and mid-IR spectra of shocked air in thermal equilibrium at temperatures of 3000, 4500 K, and 6000 K. This detail shows part of the fundamental vibrational band of NO at 5 micron and the first overtone.

Figure 1b (right). As Fig. 1a. This detail shows the CN Red band and the N_2 (1+) band at 3000 K and 4500 K.

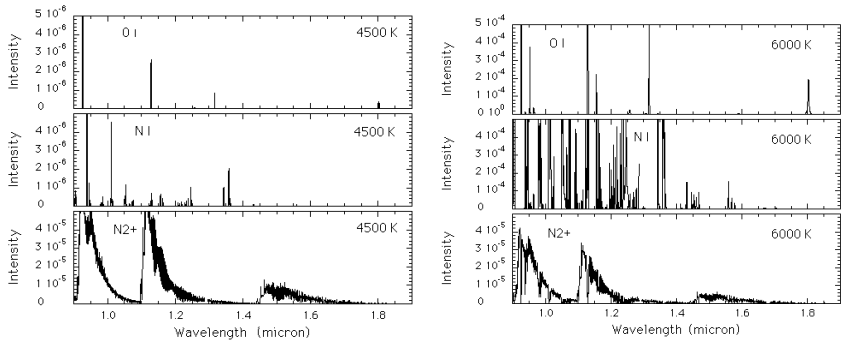

Figure 1c. As Fig. 1a. This detail shows the N2+ Meinel (1-) band at 4500 K, and lines of neutral O and N atoms

Figure 1d. As Fig. 1c - for T = 6000 K.

become detectable. At 6000 K the spectrum is dominated by N and O lines (Fig. 1d), and the spectrum has weak contributions from the N_2^+ Meinel and N_2 (1+) bands.

The bound-free continuum radiation was not evaluated. The free-free radiation comes mainly from free electrons interacting with neutral atoms in our temperature range. At 1 atmospheric pressure and temperature approaching 800 K, measurements (Laux et al. 1995) show that the free-free emission is of the order of magnitude or smallerthan the bound-bound radiation. However, free-free emission scales with the density of electrons times the density of atoms, hence with density squared, while the bound-bound radiation scales with the density of atoms only. Since at 95 km we are 6 orders of magnitude below atmospheric pressure, and taking into account the fact that the mole fraction of electrons is about 100 times larger than at 1 atmosphere, we conclude that the free-free emission at 95 km altitude, below 10,000 K, will be at least four orders of magnitude weaker than the molecular and atomic emission.

The far-infrared spectrum is expected to be dominated by the emission of OI at 63 micron because of the high abundance of atomic oxygen. This is a potentially important cooling line. No molecular bands are expected to be as strong. The dust continuum emission is expected to peak at longer wavelengths when the dust cools.

2.3. VLF EMISSIONS AND SHOCKS

Of some interest are also reported emissions of meteors at very low radio frequencies (VLF). These electromagnetic signals with audible frequencies are thought to be generated during fragmentation of meteoroids big enough to develop a shock, and the resulting sudden expansion of the meteoric plasma. The VLF signals have been linked to audible hissing sounds (electrophonic noises) that can be created by transduction of the electromagnetic signals in the environment of the witness (Keay 1993). Electrophonic noises are typically heard at the same time that the meteor is seen. However, there is no strong evidence for a direct link at present and no such records exist for Leonid fireballs.

Note that Leonid fireballs do not penetrate deep into the atmosphere (see below) and their shock waves are thought to not penetrate deep into the Earth's atmosphere also, because the excess pressure created by the flash heating along the fireball trajectory is quickly lost by radiative cooling and upward gas flow. No sonic booms are expected to be heard at the ground. However, attempts could be made to measure the possible penetration of shock waves to lower altitudes for Leonid fireballs from aircraft and high altitude balloons.

3. Meteor magnitude distribution and meteor flux

3.1. METEOR MAGNITUDE DISTRIBUTION

The intensity (I) of a meteor at a given wavelength or in a spectral band is expressed in magnitude (m):

$$m = -2.5 \log (I) \qquad (1)$$

Hence, a decrease in intensity by a factor of 100 corresponds to a change of +5 magnitudes.

The cumulative distribution of magnitudes is shown in Figure 2a. The magnitude distribution index (_) is the number ratio of meteors of magnitude m+1 and m, after correction for detection efficiency (Jenniskens 1994):

_____ = n(m+1)/n(m) (2)

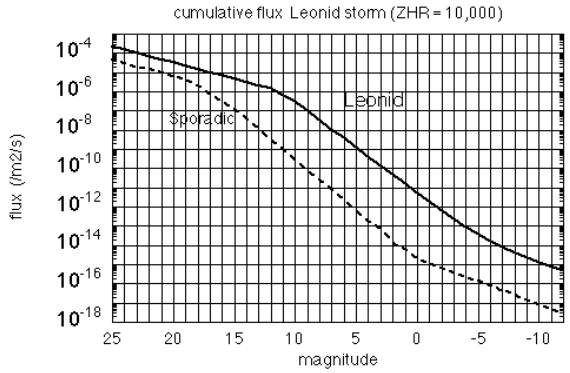

Figure 2a. The Leonid cumulative flux at the peak of a storm with ZHR = 10,000, on top of a 1997-like outburst rich in bright meteors. Dotted line is the sporadic background flux compiled by Ceplecha (1992).

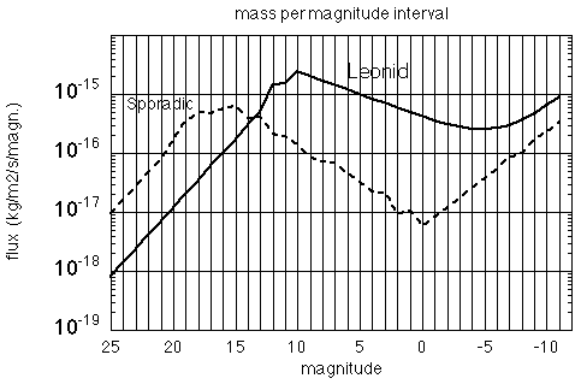

Figure 2b. As Fig. 2a. The mass per magnitude interval of Leonids and sporadic meteors.

For the visually observed Leonids during past meteor storms: $\chi = 3.0$ (McIntosh and Millman 1970, Jenniskens 1995). Hence, with each brighter magnitude class, the number of meteors drops by a factor of 3.

Fig. 2 compares the rate of Leonids at various magnitudes with the mean yearly sporadic meteor influx compiled by Ceplecha (1992) (dotted line). The typical magnitude distribution index of sporadic meteors at visual magnitudes is $\chi = 3.4$ (Kresáková 1966).

For meteors fainter than about +8, the Leonid meteor brightness distribution is expected to level off (Hajduk 1986). During the 1966 storm, a value of $\chi = 1.9$ was found by Simek and McIntosh (1968) from high power radar counts of meteors near the detection limit. That limit is at about m = +12 to +14 magn. for sporadic meteors, but probably less for Leonids. Hence, the turnover may be as shown in Fig. 2a, but could also be at somewhat lower magnitude. That would affect the rate of faint meteors. If this distribution is correct, then he Leonid flux will be orders of magnitude over the sporadic flux for all meteors brighter than +16 magnitude.

For very small particles <<10 micron, the distribution should fall off steeply because small enough particles are thought to be blown out of the stream by direct light pressure and solar wind corpuscular pressure. On longer timescales, the small particles in a stream are also depleted by the Poynting-Robertson effect, by impact erosion, collisional fragmentation, corpuscular sputtering, (e.g. Hajduk 1991) and thermal stress. On the other hand, some of these processes can generate small particles, which might steepen the size distribution.

At some high mass, the distribution should fall off too. The upper limit is set by the largest boulders that can be lifted off the comet nucleus by the evaporating water (Whipple 1951). That upper limit is thought to correspond to about -12 magn. (20 cm) for the comet's nucleus radius of R = 1.8 km (Hainaut et al. 1998), and scales with R^{-1}. It is not possible, to observe the magnitude distribution down to -12 magnitude from one given location on Earth. The local horizon limits the effective surface area that is monitored. At the Earth's surface, that limits the brightest Leonid that can be expected over the cause of the storm to about magnitude -9. At the same time about 4 meteors of -8, 13 of -7, 39 of -6 and 280 of -5 can be expected. Of course, at any given site brighter Leonids may be observed incidentally if they are present in the stream.

3.2. MASS DISTRIBUTION

The calibration of mass (M) and luminosity (m) is uncertain. Jacchia et al. (1967) derived a relation:

$$\log M\,(g) = 5.15 - 0.44 * m_{ph} - 3.89 \log V_\infty\,(km/s) - 0.67 \log(\sin(hr)) \qquad (3)$$

with hr the radiant altitude, V_∞ the apparent velocity and m_{ph} the photographic magnitude of the meteor. A colour correction described the definition of m_{ph} in comparisson to visual magnitude (m_v): $m_v = 0.71\ m_{ph} + 1.30$ over the interval for which these relations are derived ($-0.5 < m_{ph} < 2.5$ magn.). This translates to:

$$\log M(g) = 6.06 - 0.62\ m_v - 3.89 \log V_\infty - 0.67 \log(\sin(hr)) \qquad (4)$$

However, the 0.62 dependence is an unlikely artefact of a changing physical mechanism of ablation in the small magnitude range where the relationship was determined, where it changes from collisional to shock induced. Over a wider mass

range, we assume that luminosity is a constant fraction of kinetic energy. Ignoring the altitude dependence (assume hr = 45°):

$$\log M\,(g) = \log M(0) - 0.4 * m_v \qquad (5)$$

with M(0) = 0.07 gram for Leonids. For sporadic meteors, a zero magnitude meteor is about 5 gram if we assume the mean apparent velocity from the sporadic meteor distribution weighted by kinetic energy (i.e. V_∞ = 25 km/s, McDonnell et al. 1996).

3.3. METEOR FLUX

The curves in Fig. 2a give the cumulative incident rate of meteors on a 1 m^2 surface area of the atmosphere per second up to the given limiting magnitude. The sporadic flux curve is a compilation of Ceplecha (1992), Love & Brownlee (1993) and recent Eureca data by McDonnell et al. (1996), and consistent with the visual sporadic meteor flux of Jenniskens (1994).

Leonid shower fluxes are usually expressed in Zenith Hourly Rate (ZHR), the frequency of meteors visible by a standard visual observer under dark and clear skies with star limiting magnitude Lm = 6.5. Convergence factors from ZHR to other measures of influx are (Jenniskens 1994):

$$F(0) = ZHR * (0.4 + 0.6*\chi) / (30 * 7.7x10^{10} * 3600) \qquad (6)$$

Hence, for ZHR = 10,000 we have F(0) = 2.6 x 10^{-12} meteors s^{-1} m^{-2} $magn^{-1}$, when the radiant of the shower is in the zenith.

TABLE 3. Cumulative number and mass influx

	Leonid storm			Sporadic Background			
m_v	diameter	flux	mass	diameter	flux	mass	Technique
	Leonid[1]	Total storm[2]		Sporadic[3]	Daily Sporadic[4]		
magn.		(m^{-2})	($kg.m^{-2}$)		(m^{-2})	($kg.m^{-2}.day^{-1}$)	
< -4	2 cm	4 e-10	2 e-11	9 cm	2 e-11	1.3 e-10	fireballs
< 0	0.6 cm	2 e-8	2 e-11	3 cm	2 e-10[5]	1.4 e-10	photography
< +5	1.1 mm	5 e-6	4 e-11	0.5 cm	6 e-8	1.5 e-10	visual
< +8	0.4 mm	1 e-4	5 e-11	2 mm	2 e-6	2 e-10	video

[1] Spherical grain with dopted density: 0.5 g/cm^3 (log(m(g)) = -4 to +1), 1.0 g/cm (-8 to -4), 1.5 g/cm^3 (-8 to -11) (McDonnell et al. 1996; Millman 1973).

[2] ZHR_{max}=10,000 (0.7h Teff), background ZHR_{max} = 1500 (3.5h Teff)

[3] Assumed: magnitude 0 meteor = 0.07 gram (Leonid) or 5 gram (sporadic, with average 25 km/s entry velocity). Also: mass ~ $m_v^{-0.4}$

[4] in absence of impacts of masses m_v < -12 magn.

[5] 7e-10 (Millman 1975).

< +13	100 µm	8 e-3	9 e-11	400 µm	1 e-3[6]	3 e-10	radar
< +18	20 µm	6 e-2	9 e-11	80 µm	0.2[7]	5 e-10	IDP
< +25	2 µm	0.9	9 e-11	8 µm	4[8]	5 e-10[9]	spacecraft

Now, the rate of meteors in any other interval of one magnitude in the range -10 < m < +6 is calculated from:

$$F(m) = F(0)\,\chi^{m} \quad (7)$$

The cumulative flux up to a given brightness limit is summarized in Table 3. To make comparisson with sporadic influx easy, we integrated over the whole Leonid storm profile, assuming ZHR_{max} = 10,000 and an equivalent duration of 0.7 hours for the main peak and ZHR_{max} = 1,500 and an equivalent duration of 3.5 hours for the background (Fig. 3 - see below). The sporadic influx is expressed as a daily influx and strictly is the mean yearly influx to Earth.

What makes the Leonids bigger than life is the increase of rates at visual magnitudes. A factor of 1000 increase in the meteor flux transforms the shower from a dull spectacle to an impressive event. That relative increase in flux is present for all magnitudes < +7 magn., and perhaps as high as <+16 magn. The relative increase in rates is less striking for fainter magnitudes. Note, however, that this is not true for the subclass of sporadic meteors with V_∞ > 60 km/s, which is less than 1% of the total. During a storm, that fraction will increase significantly.

The storm does not last very long, with only about 3900 s equivalent duration, and the flux will fall below sporadic rates for fainter magnitudes. Integrated over the whole flux profile, the meteor flux over all magnitudes will be only equivalent to 5 hours of sporadic rates. However, the rate of observable meteors by visual observers (mv < +6 magn.) is equivalent to 2000 hours of sporadic activity. The number of fireballs (mv < -4 magn.) is equivalent to 460 hours of sporadic activity. Moreover, many of these Leonid fireballs have long-lasting trains, at much higher abundance than sporadic fireballs.

Figure 2b shows the incoming amount of matter for each magnitude interval. Most matter is expected to come in at about +10 magnitude (200 micron grains). That puts the mass peak within the range of instrumental techniques. The sporadic mass peak, on the other hand, peaks at about +16 magnitudes (150 micron grains), below the limit of existing radar techniques. Integrated over the whole flux profile, the mass influx of Leonids equals only about 4 hours of sporadic meteor influx. That matter of mainly +10 magnitude Leonids is deposited at altitudes between 103 and 98 km. This is about 15 km higher in the atmosphere than the ablation of +16

[6] 9e-5 (Love & Brownlee 1993, Grün et al. 1985).
[7] 0.06 (Millman 1975); 0.17 LDEF (McDonnell et al. 1996)
[8] 4.3 Fechtig (1973); 0.5 (Love & Brownlee 1993); LDEF: 6 (McDonnell et al. 1996)
[9] 2 e-10 for mv > 10 (Love & Brownlee 1994) - we have 4 e-10.

sporadic meteoroids, whose matter is deposited in the range 85-90 km. The peak of the sporadic neutral atom debris layer is usually near 89±3 km. This makes it possible to follow the deposition of a neutral atom debris layer and its evolution in time, especially for those neutral atoms that have a lifetime of 4 hours or less.

4. Visibility of the storms

4.1. THE RADIANT AND ORBIT

All meteors will move near parallel in very similar orbits (Table IV) before entry into the atmosphere. Hence, all meteor trails at a given time are parallel paths in the atmosphere, with an orientation moving away from the celestial equatorial coordinates Right Ascension (RA) = 153.63±0.11º, Declination (DEC) =+21.97±0.03 º (J2000). That direction is called the radiant of the shower and the radiant of the Leonid meteors is in the head of the constellation of Leo.

The Leonid radiant was measured during the 1995 Leonid outburst (Betlem et al. 1997). This position strictly refers to the "Leonid Filament", a one-day wide dust structure rich in bright meteors. The meteor storms are due to a different, more narrow structure, a 1-2 hour wide dust sheet rich in faint meteors. The storm radiant is expected to be less than a few tenths of degree from this position, however. Note that the radiant is not fixed with respect to the stars, but shifts by +0.99 ˚/day in RA and -0.36 ˚/day in DEC due to the curved path of the Earth around the Sun.

TABLE 4. Orbital elements of Leonid meteors and the parent comet (J2000).

	q (AU)	1/a (AU)	e	i ˚)	ω ˚)	Ω ˚)
Comet 55/P T-T*	0.977	0.097	0.905	162.5	172.5	235.258
Leonids 1995**	0.984	0.068	0.933	162.2	172.6	235.22
	±0.000	±0.027	±0.027	±0.1	±0.4	±0.29
Annual Leonids	0.985	0.067	0.934	162.5	173.1	235.6
	±0.002	±0.088	±0.086	±0.9	±2.5	±1.1

Notes: q = perihelion distance, a = semi-major axis, e = eccentricity,
i = inclination, ω = argument of perihelion, Ω = ascending node, equinox J2000.
* Epoch 1998, March 5.0 UT.
** Cluster of Leonid orbits observed during 1995 outburst (Betlem et al. 1997).

The pre-atmospheric apparent speed of Leonid meteors is V_∞ = 71.7 ± 0.5 km/s. The observed speed is similar, because the deceleration in the period before the

meteoroid is completely evaporated is modest, with V_∞ - <V> / <V> of order 0.2-1.5% for meteors of magnitude 0 to -4, and less for fainter meteors.

The dispersion in these parameters is expected to be very small, perhaps reflecting only the ejection velocities. In that case, the dispersion in speed could be as small as ΔV_∞ < 10 m/s, and the dispersion in radiant as small as DRA < 0.01˚. A -1 magnitude meteor ($\beta = 3.\ 10^{-4}$) is thought to have an ejection velocity of about 7 m/s.

4.2. THE INFLUX OF METEOROIDS

Figure 3 shows how the Leonid flux is expected to vary during the night of maximum activity in the best of circumstances, based on the performance of the Leonid stream in past returns (Jenniskens 1996).

The times of Fig. 1 refer to the return in 1998. The peak of the Leonid storm is expected to occur around the time of passage of the comet node, which will happen

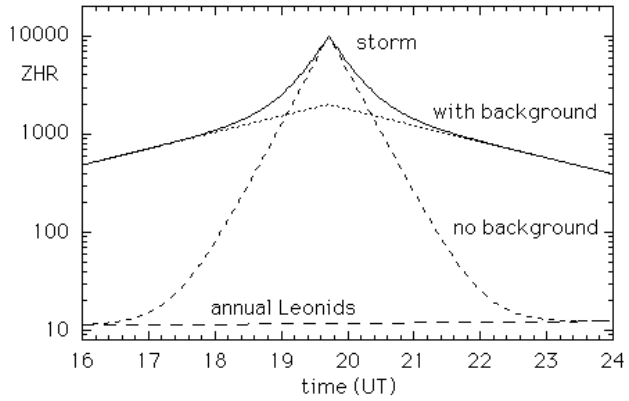

Figure 3. The expected variation of the meteor rates during the Leonid storm of 1998 (1999: about +6 h), for an assumed peak zenith hourly rate of ZHR = 10,000 (best case scenario) and a peak at the time of passing the comet node.

at 19.7 h UT on November 17, 1998, and six hours later in 1999. An uncertainty of at least ± 2 hours should be allowed for, perhaps as much as 17-23h UT.

The activity profile of the Leonid storm in Figure 3 consists of two components: a main peak and a background. The relative contribution of both has varied in the past, with a strong background in 1866 and 1901 and an almost absent background in 1966. The shape of the activity curve is expected to be similar in both 1998 and 1999, although the peak rate and time of maximum will vary.

If the peak rate is ZHR = 10,000, then it follows from Fig. 3 that rates in the main peak may be above 1,000 per hour for 1.6 hours and above 100 per hour for 3.3

hours. If the background component returns as strong as detected in the past, then rates could be above 1,000 per hour for a period of about 4 hours. In comparison, the normal sporadic rate is 10 per hour and the most intense annual stream (the Quadrantids) has ZHR = 130 (Jenniskens 1994).

4.3. THE APPARENT FLUX

When selecting an observing site, one has to keep in mind that the storms do not last very long. The best locations on Earth is where the radiant is high above the local horizon at the time of the storm and where it is still night time.

The observed flux of meteors depends on the angle of incidence of the meteors, which is the radiant elevation (hr) above the horizon. Best fluxes are observed when the angle of incidence is high. If the meteors are not coming from the zenith (hr = 90˚) but at an angle hr < 90˚, then the flux is diluted over a larger surface area of the atmosphere, and the observed hourly rate (HR) is:

$$HR = ZHR * \sin(hr)^{\gamma} \qquad (8)$$

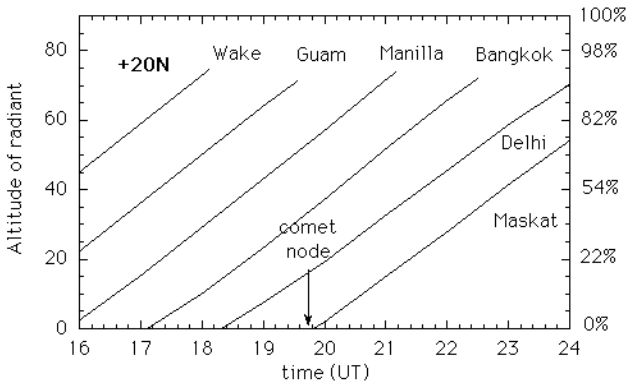

Figure 4a. Visibility of Leonids in 1998 from locations at around latitude +20N

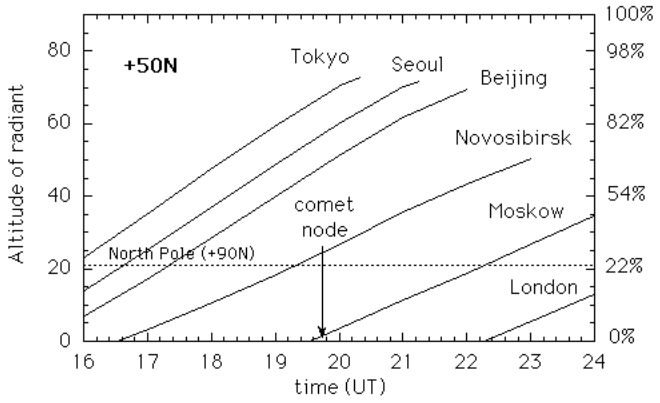

Figure 4b. As fig. 4a. For locations at about latitude +50 N

with $\gamma = 1.0$. The observed flux is also dependent on the increase of trail length and apparent angular velocity and decreasing meteor brightness with increasing hr, which causes γ to be typically larger than 1. For fast Leonids, γ may be in the range 1.0 - 1.8 (Bellot Rubio 1995). We will adopt $\gamma = 1.4$ as in Jenniskens (1994).

Figures 4a and 4b are two examples of how observing conditions vary with latitude and longitude. The figures show the altitude of the radiant around the time of the predicted return for various locations at +20 N and +50 N latitude respectively. The right axis gives the radiant altitude, while on the left axis is given to what level the incident ZHR is diluted. At each location, the visibility is limited by the time that the radiant rises above the horizon and the time that the shower is lost at dawn, which for most purposes is the beginning of Nautical twilight. If the meteor observing technique allows daylight observations, then the observing interval extends into daytime until the radiant sets around local noon (+20 N).

We find that if the peak is at 19.7 h UT and the observer is at +20 N latitude, then the radiant will be below the horizon westward of Maskat, while the storm will be lost in daylight for locations west of Guam. At each location, the observing interval will only be about 5.5 hours. Going further north (+50 N) will increase the observing interval because the Sun rises later, but the average radiant altitude is lower (also, north of Beijing the ground temperature is expected to drop below freezing at night). Going further south than +20 N is not recommended, because it will not only decrease the mean radiant altitude, but it will also decrease the observing interval. A different perspective is given in Fig. 5, which shows the Earth as seen from the perspective of approaching Leonid meteoroids at the time of the nodal passage.

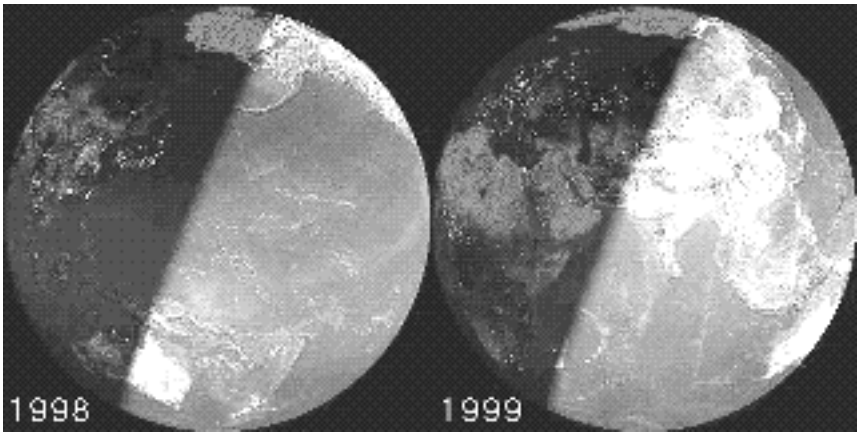

Figure 5. The Earth as seen from the approaching Leonid meteoroids at the time of the nodal passage in 1998 and in 1999

4.4. ATMOSPHERIC CONDITIONS

In many situations, the visibility is also limited by the local weather conditions, which will not be discussed here. It is sufficient to say that November weather is notoriously bad at most parts of the Northern Hemisphere and it is impossible to find a ground-based observing location which guarantees clear weather. It serves as a warning that during the previous return in 1966 all professional attempts to collect data from ground-based observing sites (in the US and Canada) failed due to such unforeseen weather conditions (except for radar studies, that is, which are generally unaffected by clouds).

Of concern are also cirrus clouds and other forms of haze (fog, smog). Scattering of light by ice crystals, water droplets or dust increases the total extinction in any given direction above the amount caused by Raleigh scattering off the atmosphere's molecules. To illustrate the magnitude of the effect, it suffices to point out that a decrease of one magnitude in the transparency of the atmosphere means a decrease by a factor of χ (~3.0) in the number of observed Leonids, whereby χ is the magnitude distribution index.

4.5. THE MOON.

Moonlight also lowers the rate of observed meteors for many optical observations by increasing the sky background brightness and, therefore, decreasing the star limiting magnitude. Fortunately, the near new Moon (28 days) will not disturb in 1998, while a first quarter Moon (10 days) in 1999 will set shortly after the radiant of the stream rises above the horizon.

The brief interval with high meteor rates and a Moon above the horizon may allow direct observations of impacting Leonids on the Moon in 1999 for locations that are west of the night-time part of Fig. 5. Effects on the Moon's sodium atmosphere

might be seen in the days following the Leonid storms. In 1998, that would demand observing the Moon at low altitude above the horizon, which will need clear atmospheric conditions. In 1999, the Moon can be observed at selected locations at the time of the event.

5. Manifestation of Leonid meteors on the sky

5.1. METEOR RATES

We will now turn to how the Leonid shower manifests on the sky. The number density of Leonids on the sky in a certain viewing direction is determined by the effective surface area for a given field of view, and the decrease of meteor brightness due to atmospheric extinction and due to the distance between viewer and meteor.

The distance (d) to the meteor level at height H in a viewing direction h degrees above the horizon, for an Earth radius R = 6370 km and a curved atmosphere (Koschack and Rendtel 1990):

$$d = R + H \sin \left(\arccos \left((R \cos h) / (R + H) \right) - h \right) / \cos h \qquad (9)$$

The increase of rates for an increasing effective surface area per square degree on the sky is proportional to:

$$n(m) = F(m) \ (d/H)^2 \qquad (10)$$

Typically rates change with changing apparent magnitude (Δm):

$$n(m) = F(m) \chi^{-\Delta m} \qquad (11)$$

The decrease in brightness due to distance is:

$$\Delta m = -5 \log (d / H) \qquad (12)$$

The extinction correction includes Raleigh scattering (k_r) and scattering by dust and ice particles on hazy days (k_d). Typically (Siedentopf and Scheffler 1965):

$$\Delta m = (k_r + k_d) / \sin (hr) \qquad (13)$$

where k is the extinction coefficient. k is wavelength dependent. For extremely clear weather high in the mountain, $k_r = 0.099$ and $k_d = 0.024$, hence $k = 0.123$ at 5500 Å, relevant to visual observations (Sidgwick & Muirden 1980).

Figure 6 (top, left) shows the resulting distribution of meteor rates n(m) on the sky, in arbitrary units. These diagrams are to be read as follows. Each number is for a viewing direction differing by 10˚ from the neighboring positions. The center number is that for the zenith, the point straight above the observer.

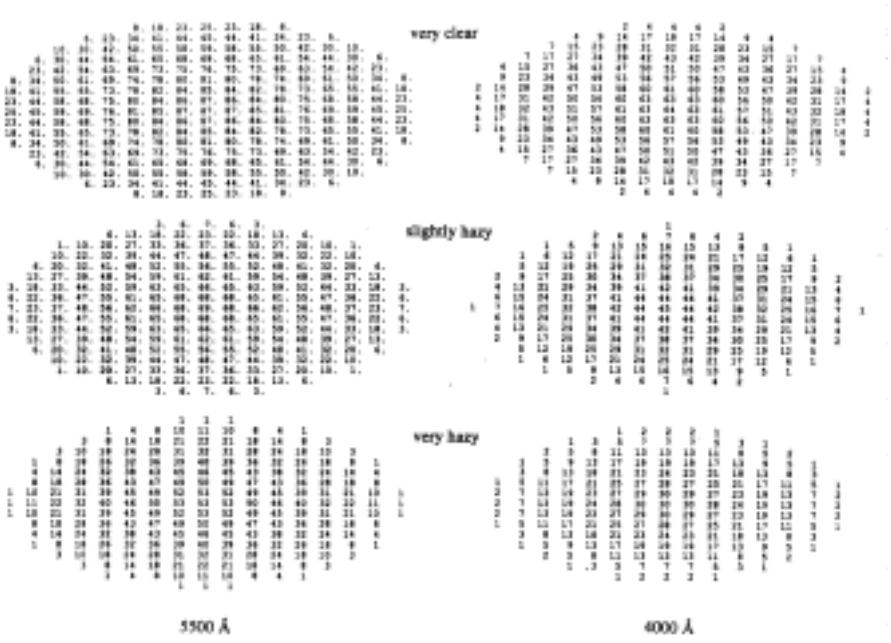

Figure 6. The number density of meteors in arbitrary units for viewing directions differing by 10˚ on the sky. From top to bottom: total extinction k = 0.123, k = 0.40 and k = 0.84

From Fig. 6 it follows that in very clear conditions, the number density of meteors on the sky is almost constant for viewing angles above 30˚ elevation, falling to only 32% of the flux in the zenith. If observing conditions are not perfect, k_d quickly increases. For a clear day at the ground, for example, $k_d = 0.118$ at 5500 Å, while for a day with slight haze $k_d = 0.236$ and for a very hazy day $k_d = 0.471$. From top to bottom is shown how the meteor distribution on the sky changes as a result of increasing hazy conditions. When the amount of haze increases, the highest meteor rates are seen higher in the sky.

The total extinction also varies strongly as a function of wavelength. Typically, k decreases with increasing wavelength in the visual and near-infrared, but can be high in wavelength ranges where atmospheric bands absorb. The higher the expected extinction, the more the observing strategy demands a high aiming point in the sky. For example, for photographic techniques sensitive to emission in the near-UV, where the meteors are bright, the relative wavelength is about 4000 Å. At 4000 Å, Raleigh scattering is as intense as $k_r = 0.367$ while dust extinction adds $k_d = 0.036$,

or k = 0.40. Figure 6 (right) shows the resulting distribution of n(m) for the same observing conditions as above.

5.2. TRAIL LENGTH (METEOR DURATION)

The meteor trail length is of interest in imaging techniques, because for many purposes it is necessary to capture the whole meteor train in the field of view. The trail length also determines the detection efficiency at any given part of the sky: by suitably orienting the field of view with the short axis towards the radiant, one can maximize the detection efficiency. Also, the trail length is directly proportional to the duration of the meteor, because the deceleration of the meteor is small. And the duration of meteors affect the accuracy of the velocity determination in multi-station imaging. Typically, the longer the meteor persists, the more accurately the velocity can be measured.

The measured trail length is a function of the detection threshold and differs for video and photographic observations. The beginning of the trail is affected mostly. That is because the meteor intensity increases gradually, while fading relatively rapidly.

We obtained measurements of Leonid trajectories from both photographic and video techniques during the 1995 Leonid return (Betlem et al. 1997). 22 meteors were photographed and 13 were recorded by image intensified video systems. Figures 7a and 7b summarize the height of beginning and end of the trajectory as a function of zenith distance of the radiant ($Zr = 90^\circ - hr$) and absolute visual magnitude (m). The two effects were deconvolved by correcting the heights to the lsqfit value at m = 0.0 and cos (Zr) = 1. It is these values that are shown in Fig. 7.

We find that photographic and video techniques result in the same dependence of the end height as a function of brightness and zenith distance:

$$He = 93 + 1.3\ m \tag{14}$$

$$He = 93 - 6.0 \sin (hr) \tag{15}$$

The beginning height is a strong function of meteor brightness in the video records, but much less so in the photographic records. The beginning height of magnitude 0 meteors in the video record is about 35 km higher than in the photographic record. The latter technique is much less sensitive, implying that Leonids brighten very gradually, but fade rapidly.

Of particular interest are also the video observations of two bright 1996 Leonid fireballs of -7 and -4 magnitude by observers of the Nippon Meteor Society, which had a beginning height around 160 km. This is consistent with the observed trend here (Fujiwara et al. 1998). That implies that the full range of meteor atmosphere that can be studied by Leonid meteors is between 160 and 85 km! The high beginning heights are only understood if some material is sputtered that has low sublimation temperature (e.g. kerogens or amorphous carbons). Hence, spectroscopy of these high altitude emissions offer an opportunity to study the organic component of meteoroids. Although the beginning height is different for video and photographic

meteors, we find that the duration (Δt) of the video and photographic meteors have the same dependence on the zenith distance of the radiant (Fig. 8):

$$\Delta t \sim \sin (hr)^{-1.1\pm0.1} \qquad (16)$$

Hence, the duration of Leonids is a factor of two larger if the radiant is at 32˚ than when the radiant is in the zenith, a factor of 4 at 16˚, and a factor of 8 at 9˚.

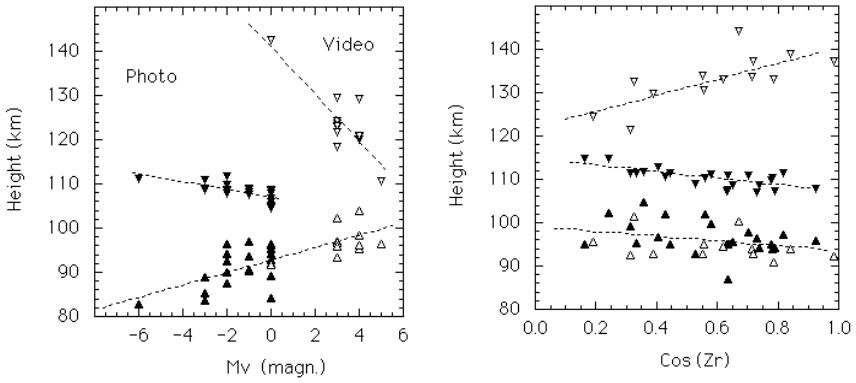

Figure 7a. The beginning and end heights of Leonid meteors as a function of Leonid meteor magnitude (for a radiant in the zenith). Closed symbols: photographic data; open symbols: video data. Dashed lines are least-squares fits through the data.

Figure 7b. As Fig. 7a. As a function of the zenith distance of the radiant (Zr = 90˚ - hr), for Leonid meteors of magnitude 0.

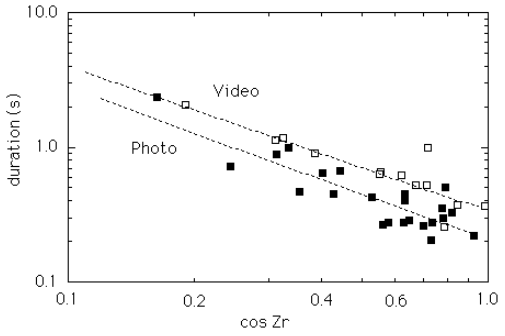

Figure 8. The duration of Leonid meteors as a function of zenith distance.

With the above relationships for the end height, we find that the trail length of magnitude 0 meteors (photographed by small 35 mm f1.8/50mm cameras with 400 ASA black and white film) is given by:

$$l = 15.0^{\circ} \sin(hr)^{-1.1\pm0.1} \quad (17)$$

while the variation as a function of viewing angle and radiant altitude (hr) is shown in Fig. 9. The radiant is in a direction right of center in these plots. The trail length of Leonids at other magnitudes or observed with video instead of photographic techniques scales according to dependencies in Fig. 7.

The trail length typically increases further away from the radiant and further away from the horizon. The longest trails are measured when the radiant altitude is about 30 degrees, not far from the zenith in a direction opposite the azimuth of the radiant. The trail length typically decreases with decreasing brightness of the meteor (increasing magnitude).

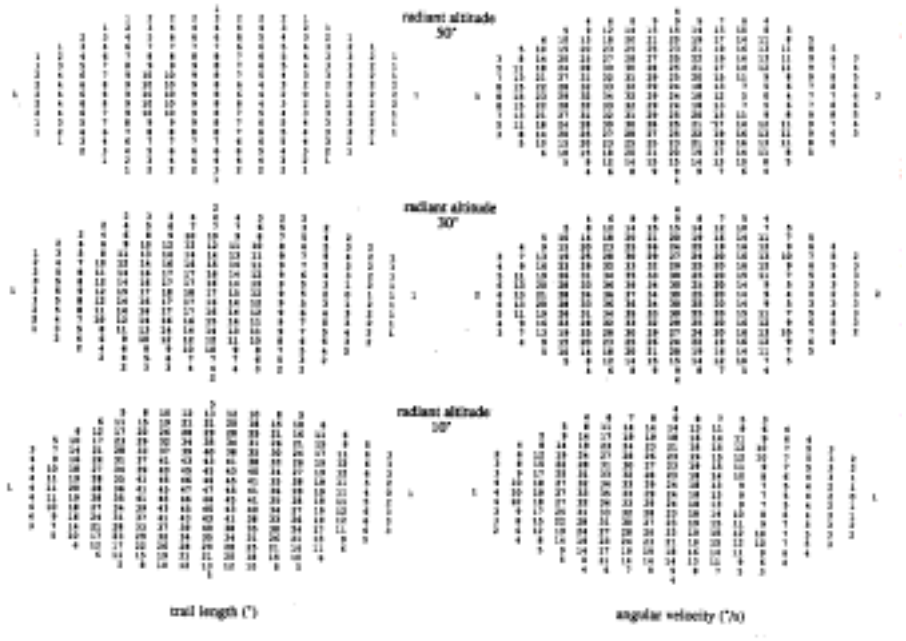

Figure 9. Trail length (left plots) and the angular velocity (right plots) of Leonid meteors as a function of the viewing direction in the sky for various radiant altitudes

5.3. ANGULAR VELOCITY

Of particular interest is also the angular velocity of the Leonids in various viewing directions. The angular velocity determines the time the meteor signal crosses one pixel on a detecting element.

For a trail length l (km), distance to the meteor level d (km) and an angular distance from the radiant De:

$$\omega = l / \sin(l) * v_\infty / d * \sin(De - l) \sim 57.3^\circ * 71.7 * \sin(De - l) / d \quad (18)$$

where De follows from (for azimuth viewing direction az, and azimuth of radiant azr):

$$\cos De = \sin hr \sin h + \cos hr \cos h \cos(az - azr) \quad (19)$$

Even though all meteors enter at around V_∞ = 72 km/s, the angular velocity of the meteor on the sky varies considerably. Not all meteors appear "very fast". When viewing in a direction towards the radiant, in a direction De = 0˚, the meteors move towards the observer and appear as a point source. Close to the radiant the meteors are foreshortened and move at a very low angular velocity. Meteors low on the horizon are far from the observer, and they too appear to move relatively slow. The radial velocity peaks for viewing directions close to De = 90˚. The right figures of Fig. 9 give the radial velocities (in degrees per second) calculated for an end height as shown in Fig. 7, and a trail length as indicated by the duration in Fig. 8.

Note that for some applications viewing directions perpendicular to the radiant are preferred (e.g. astrometry for highest positional and velocity accuracy), while other techniques benefit from observing directly towards the Leonid radiant (e.g. radar and LIDAR ranging techniques).

6. Manifestation of persistent trains

6.1. NATURE OF PERSISTENT TRAINS

The Leonids are unique among meteor streams by the large number of long-lasting persistent trains that are produced. Leonids of magnitude -4 or brighter are known to produce such trains (e.g. Baggaley 1978). One -6 Leonid produced the train shown in Fig. 10, which was observed during our 1995 Leonid campaign over California (Betlem et al. 1997). The train was visible by naked eye for 6 minutes after the meteor had vanished.

During an effort to observe such a Leonid train using the CAT telescope at ESO, LaSilla, in November 1996, we observed the following brightness evolution of a train that occurred almost in the zenith. First, the meteor persistent train rapidly decayed from about +1 to +3 magnitude in about 10 seconds. The emission during this decay is probably due to the green forbidden line of oxygen OI at 5577 Å (Borovicka et al. 1996). During this phase, the train rapidly expands due to thermal expansion until it achieves pressure equilibrium with the surrounding atmosphere. During expansion, one can observe some wrinkling and small scale distortions due to instabilities and turbulence. Any structure rapidly fades into a diffuse beam of light that splits in two parallel beams. This is the stage where the emission decay halts and stays constant for as long as 6 minutes for a -5 Leonid, up to half an hour

or so for brighter Leonids. Finally, the train intensity suddenly drops and even with binoculars no trace can be observed after this collapse.

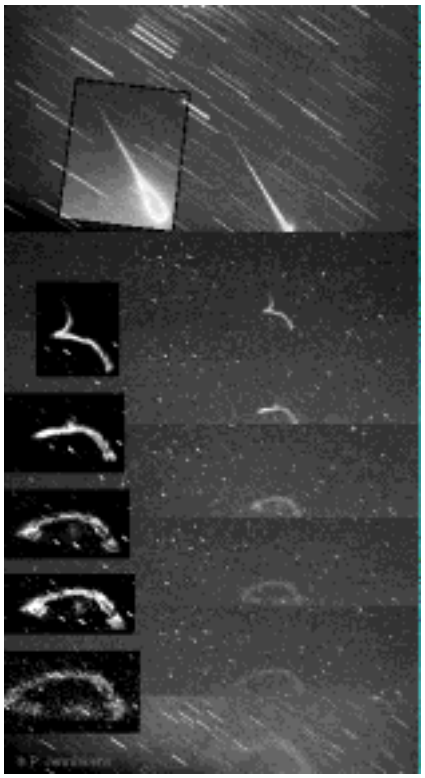

Figure 10. Long lasting persistent train observed in California on November 18, 1995. The meteor appeared at 11: 45:22 UT. A persistent train was visible with the naked eye for 6 minutes. The train was photographed in a series of 1-minute exposures starting at 11:45:59, 11:46:59, 11:47:59, 11:49:06, and 11:50:05 UT, followed by a five-minute exposure starting at 11:51:06 UT. Note the 2-beam (hollow) structure. The inset shows the same meteor photographed from a different location.

Hence, during the persistent phase the meteor train appears hollow. The intensity is not centrally condensed. The mechanism that keeps the train luminosity high for such long period of time must involve turbulence or diffusion of hot air in the train and an interaction with the surrounding atmosphere. It is thought that metal ions may catalyze the reduction from O and O_3 to O_2: $O_3 + M > MO + O_2$ and $O + MO > M + O_2$ (Poole 1979, Baggaley 1980, Hapgood 1980), but there is no spectroscopic data to confirm that. It is this mechanism that is responsible for most of the visible luminosity. One low-resolution Perseid train spectrum is discussed by Borovicka et al. (1996).

6.2. DETECTION OF PERSISTENT TRAINS

The detectability of a persistent train depends on the surface brightness. A train in the zenith of a meteor of shallow entry angle has a surface brightness of about 13 magn/square arcseconds, or a visual magnitude of about +3. Hapgood (1980) observed a train with a video camera sensitive to a broad band in the near-Infrared between 700 and 900 nm and obtained a line emission rate 2 x 10^{17} photons s^{-1} m^{-1}.

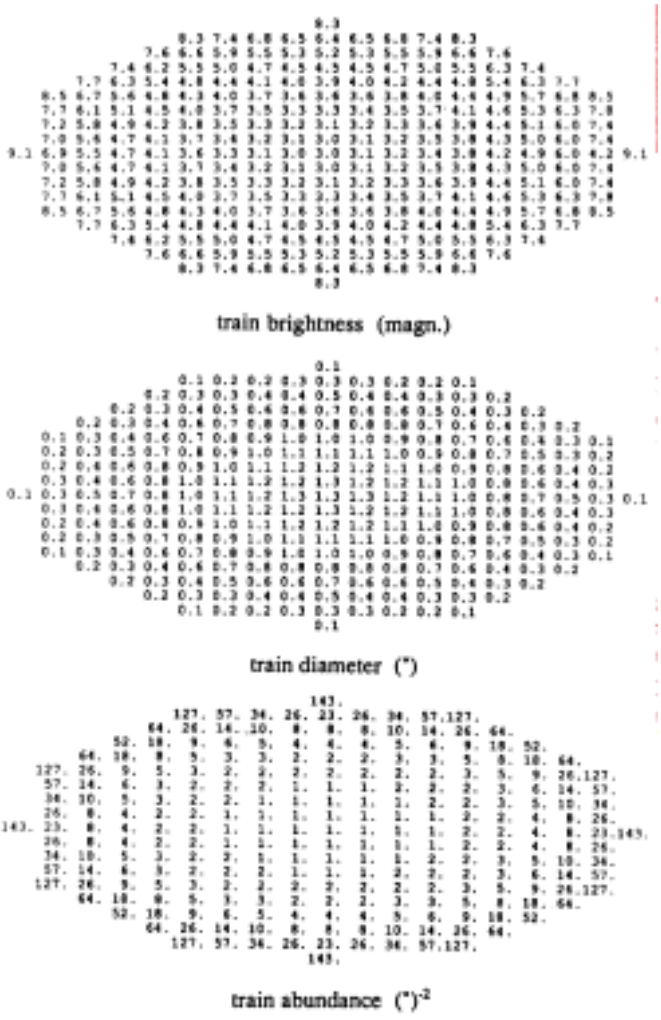

Figure 11. Train luminosity (above) and train diameter (middle) and train occurrence (below) as a function of viewing direction for a high (Zr = 0°) radiant altitude

The expected dependence of train surface brightness as a function of viewing direction is shown in Fig. 11. It is taken into account that the line of sight through the train depends on the relative orientation of the train (the angle between radiant and viewing direction). As a result, when the trains appears close to the radiant, the line of sight is along the train and it appears much brighter. Note that these brighter trains do not last longer, although in general the brighter trains are expected to do.

Of special interest is also the diameter of the persistent train, which decreases with increasing distance to the meteors (Fig. 11). The trains expand to a width of about 2 kilometers in the persistent phase (from a typical diameter of about 40 meters for trails detected by LIDAR). The train is about a degree wide when it appears high on the sky. Only below 30 degrees altitude does the train diameter decrease significantly.

Although trains tend to appear relatively low on the horizon, where the effective surface area per degree field of view is high, they are also fainter and more difficult to detect. If all Leonids of an absolute visual magnitude of -4 leave a persistent train, Fig. 11 shows how the chance of detecting a train varies as a function of viewing direction. Below 20 degrees altitude, the chance quickly increases. However, the train brightness is so much less that a typical visual observer will not be able to recognize these trains and the abundance of trains is relatively constant. The low altitude trains should be obvious, however, for more sensitive techniques. Given that persistent trains may occur for meteors of a certain minimum brightness, one has to look out for trains of a lesser brightness allowing for the attenuation due to distance and extinction. For a visual observer under clear conditions at sea level, the apparent brightness of -4 meteors in the zenith is -3 at 46˚, -2 at 29˚, -1 at 19˚, +0 at 13˚, +1 at 9˚ and +2 at 6˚.

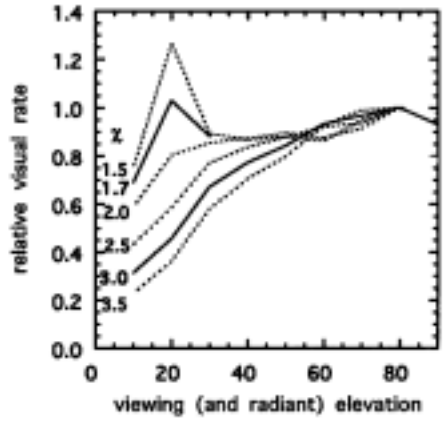

Figure 12. The observed rates as a function of magnitude distribution index χ for a visual observer watching at various elevations from the horizon

7. Applications

7.1. VISUAL OBSERVATIONS

Visual naked eye observations have a relatively wide field of view, the size of which is strongly dependent on meteor magnitude. Part of the field of view is obstructed by the horizon. As a result, the detection rate depends in a complicated way on the viewing direction.

In order to calculate the observed rate as a function of viewing elevation (h), we calculated the expected flux (n) for different positions on the sky as in Fig. 6, but for an observer at sea level under clear skies (k = 0.217). We then assumed that an observer was watching towards the radiant. His or her probability of detecting a meteor of given magnitude (m) at distance (De) from the center of vision P(m,De) was taken to be the values measured by Koschack and Rendtel (1990). We then integrated this flux level over the field of view, weighting each direction by a factor that is proportional to the overall detection efficiency over the whole magnitude range:

$$HR(h) = n(h) * \Sigma m \; P(m,De) \; \chi^{-m} \qquad (23)$$

Observers tend to either concentrate on the central part of the field of view or watch over a much wider region. For the sake of illustrating one particular case, we have adopted the mean of the given values of P(m,De), neglecting a possible h-dependence. A different function was used by Van Vliet (1994), with qualitatively similar results as shown in Fig. 12.

For high χ such as during the meteor storm, the viewing direction is best above 30˚ altitude (Fig. 14). Below that, the horizon cuts off a significant part of the field of view, lowering the rates. For low $\chi < 2.0$ rates stay about constant down to 20˚ elevation and may even peak at these low viewing elevations. That is because a relatively higher fraction of meteors originates from the large effective field of view for brighter meteors. This situation is relevant for the recent Leonid outbursts of 1994 - 1996, when χ was about 1.7. However, the same will apply when observers pay less attention to the faint meteors and start noticing the bright ones by their sheer number, a situation that may well occur during the upcoming storms. Hence, the abundance of bright Leonids in the storm as remembered by the visual observer will depend much on the observing technique.

7.2. PHOTOGRAPHIC OBSERVATIONS

The detection efficiency for photographic observations scales with the flux of the meteors (Fig. 6), but also inversely with the angular velocity ω (Fig. 9).

The elevation-dependence of flux is most sensitive to the atmospheric extinction. Photographic observations are most efficient when the film is sensitive to the intense near-UV emission of the meteors. At those wavelengths, a relatively high extinction coefficient applies. k = 0.4 was adopted here to illustrate conditions typical at a wavelength of 4000 Å at the ground during a clear night.

The number of photons collected in a single pixel of the detector scales with the time the meteor image is projected on the pixel, hence inversely with ω. For a typical fast moving meteor, the effective brightness decrease is according to:

$$\Delta m = 2.5 \log (\omega / \omega_o) \qquad (24)$$

Fig. 13 shows the resulting detection efficiencies. Clearly, rates are highest near the radiant (foreshortening) and at high elevations (low extinction). The well known effect of low detection efficiencies in the direction opposite of the radiant is also apparent in the graphs of Fig. 13, and is a result of the high angular velocity.

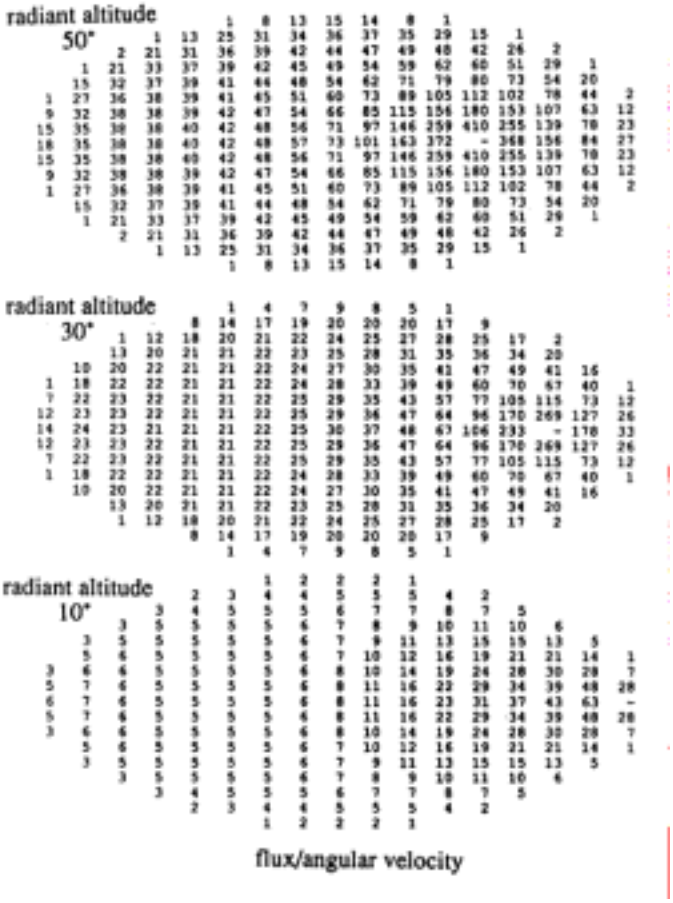

Figure 13. The detection efficiency for meteor photography (in arbitrary units) for viewing directions differing by 10˚ on the sky. From top to bottom: radiant altitudes 50˚, 30˚, and 10˚

For the purpose of measuring meteor flux, one has to keep in mind that preferentially the angular velocity should not change too much in the field of view (Bellot Rubio 1994). Hence, when aiming the cameras, it is good to avoid the radiant direction, because the angular velocity of the meteors varies widely in that direction.

7.3. NEAR-IR SPECTROSCOPY

The situation changes dramatically if the detection technique is sensitive in the near-infrared outside atmospheric absorption bands where extinction is very small. In that case the detection efficiency is almost constant over the entire sky, with only an enhancement close to the radiant direction due to foreshortening (no Figure). It was again assumed that the detection efficiency of photons per pixel is inversely proportional to the angular velocity, as for example in slit-less spectroscopy.

8. Laboratory astrophysics and space science

This paper has described some of the opportunities for remote observing of meteoroids and their interaction with the Earth's atmosphere. At the time of a meteor storm, nature offers the opportunity for a unique series of laboratory experiments with relatively well controlled parameters that are varied in ways that are inaccessible by other techniques. These include flash-heating experiments of relatively large mm-cm sized cometary materials, ultra-high-velocity re-entry dynamics, and reaction chemistry experiments involving neutral metal atom debris in the upper atmosphere. The detection techniques used will be mainly remote sensing imaging, spectroscopic, and ranging techniques in ground-based and airborne observations. Space experiments can include spectroscopy at wavelengths inaccessible from the ground, and detection of the smallest grains in the shower by impacts on foils and aerogels. In addition, balloon experiments may be able to collect the recondensed meteoric vapor or meteoric debris if it is possible to distinguish the Leonid debris from debris of sporadic meteors.

The Leonid Multi-Instrument Aircraft Campaign is an airborne laboratory, lead by NASA/Ames Research Center, that will provide a podium for an international group of scientists to be under favorable observing conditions in eastern Asia at the time of the event in November of 1998. If all develops to plan, more than ten different experiments will use imaging, spectroscopic and ranging techniques from two aircraft.

Leonid MAC will address key issues related to the composition of cometary matter, the dynamics of transport of this matter to Earth, the creation of NO and other molecules in the meteor path, neutral atom chemistry and the formation of condensables. For that purpose, meteors will be imaged for flux measurements. Slit-less UV/Vis spectroscopy will address the abundance of the main rock-forming elements, near-IR spectroscopy will try and detect the organic component in cometary matter. Meteor trains will be studied by high-resolution spectroscopy and

the visual and near-IR and by low-resolution mid-IR spectroscopy for mineralogy and the detection of an emission continuum from dust. Efforts will be made to try detect the scattered sunlight of meteoroids in space, thus measuring the scattering properties of relatively large cometary matter. Finally, lidar ranging techniques will be used to study the deposition of neutral atom debris during the shower and follow the kinetics over time in a reaction chemistry experiment.

Other experiments are planned by researchers worldwide, including ground-based radar measurements for meteor flux, multi-station photography for meteor orbits, studies of the Moon's sodium atmosphere, balloon borne and sounding rocket collection of upper atmosphere debris, and satellite impact studies.

The results of these observations will generate new opportunities for laboratory astrophysics and space research experiments during the 1999 return of the Leonids.

9. Further information

The above discourse is all but complete and other considerations, observing techniques, and targets certainly exist. However, we hope that the present information will already be of benefit to a wide range of potential observers of the Leonid meteor storms.

Further information regarding the Leonid shower and the Leonid Multi-Instrument Aircraft Campaign can be found at the website:

http://leonid.arc.nasa.gov/

We would like to end this work with a word of caution and a warning not to put expectations too high, but also not to put expectations too low. One should weight the likely outcome of various observing strategies against expected peak flux levels. Some effort has to be aimed at the best possible outcome in terms of spectral resolution, imaging, and ranging accuracy, risking no result at all, in order to be able to make full use of the high flux of meteors and meteor trains that the Leonids may offer us in November of 1998 and 1999.

Acknowledgments:

The Leonid photographic and video observations described in this paper were obtained by members of the Dutch Meteor Society in November of 1995 from locations in the south of Spain. Klaas Jobse pioneered the video observing program. We thank Westley Traub of SAO Harvard for his contribution of a study of the expected far-infrared line emission of meteor trains. The paper benefited from a validation flight with the Advanced Ranging Instrumentation Aircraft performed by the 412th Test Wing of the US Air Force 452d Flight Test Squadron at Edwards AFB in August of 1997. We thank especially Glenn Hamilton, the ARIA program manager, Steve Wenke, the senior pilot for the ARIA program, and Greg Williams, the senior optical imaging specialist. The paper also benfited from comments by referees Junichi Watanabe and Hermann Kochan. PJ is supported by the NASA Planetary Astronomy program.

References

Baggaley W.J. 1978. Meteor magnitudes and enduring trains. The Observatory 98, 8-11.
Baggaley W.J. 1980. Meteors and atmospheres. In: Solid Particles in the Solar System. IAU Symp. 90 (Halliday I. and McIntosh B.A., eds.), pp. 85-100.
Bellot Rubio R.L. 1994. Spatial Number Densities and Errors from Photographic Meteor Observations under Very High Activity. WGN, the Journal of IMO 22, 118-130.
Bellot Rubio R.L. 1995. Effects of a dependence of meteor brightness on the entry angle. Astron. Astrophys. 301, 602-608.
Betlem H., ter Kuile C.R., van 't Leven J., de Lignie M., Ramon Bellot L., Koop M., Angelos C., Wilson M., Jenniskens P, 1997, Precisely reduced meteoroid trajectories and orbits from the 1995 Leonid meteor outburst, Planet. Space Science 45, 853-856.
Borovicka J. 1993. A fireball spectrum analysis. Astron. Astrophys. 279, 627-645.
Borovicka J. 1994. Line identification in a fireball spectrum. Astron. Astrophys. Suppl. Ser. 103, 83-96.
Borovicka J., Zimnikoval P., Skvarka J., Rajchl J., Spurny P. 1996. The identification of nebular lines in the spectra of meteor trains. Astron. Astrophys. 306, 995-998.
Brown P., Simek M., Jones J. 1997. Radar observations of the Leonids: 1964-1995. Astron. Astrophys. 322, 687-695.
Ceplecha Z. 1992. Influx of interplanetary bodies onto Earth. Astron. Astrophys. 263, 361-366.
Fechtig H., 1973, Cosmic Dust in the Atmosphere and in the Interplanetary Space at 1 AU Today and in the Early Solar System. In: Evolutionary and physical properties of meteoroids, NASA-SP 319, C.L. Hemenway, P.M. Millman, A.F. Cook, eds., 209-221.
Fujiwara Y., Ueda M., Shiba Y., Sugimoto M., Kinoshita M., Shimoda C. 1998. Meteor Luminosity at 160 km altitude from TV observations for bright Leonid meteors. GRL 25, 285-288.
Grün E., Zook A.H., Fechtig H., Giese R.H., 1985, Icarus 62, 244.
Hainaut O.R., Meech K.J., Boehnhardt H., West R.M. 1998. Early recovery of Comet 55P/Tempel-Tuttle. Astron. Astrophys. (in press)
Hajduk A. 1986. Meteoroids from comet Halley and the comets mass production and age. In: Proc. 20th ESLAB Symp. on the Exploration of Halley's Comet, ESA SP-250, pp. 239-243.
Hajduk A. 1991. Mass distribution and bulk density distribution of interplanetary dust. In: Origin and Evolution of Interplanetary dust. (Levasseur-Regourd A.C., Hasegawa H., Eds.), pp. 331-334.
Hapgood M.A. 1980. IR observation of a persistent meteor train. Nature 286, 582-583.
Harvey G.A. 1973. Spectral Analysis of Four Meteors, in Evolutionary and Physical Properties of Meteoroids, NASA SP-319, (C.L. Hemenway, P.M. Millman, A.F. Cook., Eds.), pp. 103-129. NASA, Washington D.C.
Jacchia G.J., Verniani F., Briggs R.E. 1967. An analysis of the atmospheric trajectories of 413 precisely reduced photographic meteors. Smithson. Contrib. to Astrophys. 10 (1), p. 1-139.
Jenniskens P. 1994. Meteor Stream Activity. I. The Annual Streams. Astron. Astrophys. 287, 990-1013.
Jenniskens P. 1995. Meteor Stream Activity. II. Meteor Outbursts. Astron. Astrophys. 295, 206-235.
Jenniskens P. 1996. Meteor Stream Activity. III. Measurements of the first in a new series of Leonid outburst. Meteoritics and Planetary Science 31, 177-184.
Kane T.J., Gardner C.S. 1993. Lidar Observations of the Meteoric Deposition of Mesospheric Metals, Science 259, 1297-1299.
Keay C.S. 1993. Electrophonic Meteor Fireballs require further study, in Meteoroids and their Parent Bodies, (J. Stohl, I.P. Williams eds.), pp. 315-318. Astron. Inst. Slovak Acad. Sci., Bratislava.
Koschack R., Rendtel J. 1990. Determination of spatial number density and mass index from visual meteor observations (II). WGN, the Journal of IMO 18, 119-140.
Kresáková M. 1966. The Magnitude Distribution of Meteors in Meteor Showers. Contr. Ast. Obs. Skalnaté Pleso 3, 75-108
Laux C.O., Gessman R.J., Hilbert B., Kruger C.H. 1995. Experimental Studies and Modeling of Infrared Air Plasma Radiation, AIAA paper 95-2124, 30th American Institute of Aeronautics and Astronautics Thermophysics Conference, June 19-22, 1995, San Diego, CA (no bound proceedings).
Love S.G., Brownlee D.E., 1993, A direct Measurement of the Terrestrial Mass Accretion Rate of Cosmic Dust, Science 262, 550-553.
McDonnell J.A.M., Gardner D.J., McBride N., 1996, Recent near Earth satellite flux data: contributions in the definition of the interplanetary flux at 1 AU heliocentric distance. in Physics, Chemistry and Dynamics of Interplanetary Dust, B. A. S. Gustafson, M.S. Hanner eds., ASP Conference Series, 104, 193-200.
McIntosh B.A., Millman P.M. 1970. The Leonids by Radar - 1957 to 1968. Meteoritics 5, 1-18.
McKinley D.W.R. 1961. Meteor Science and Engineering. 309 pp. McGraw-Hill Book Company, New York.
Millman P.M., 1975, Dust in the Solar System. In: The Dusty Universe. G.B. Field, A.G.W. Cameron (eds.), p. 185-209.
Poole L.M.G. 1979. The excitation of spectral lines in faint meteor trains, J. of Atmosph. Terr. Phys. 41, 53-64.
Sidgwick J.B., Muirden J. 1980. Amateur Astronomer's Handbook. Fourth Ed., pp. 437-460. Enslow

Publishers, New Jersey.
Siedentopf H., Scheffler H. 1965. Influence of the earth's atmosphere. In: Landolt-Börnstein, Numberical data and functional relationships in science and technology. (K.H. Hellwege, Ed.), Sect. 1.5, p. 52. Springer Verlag, Berlin.
Simek M., McIntosh B.A. 1968. Meteor Mass distribution from Underdense Trail Echoes. In: Physics and Dynamics of meteors. (L. Kresak, P.M. Millman, Eds.), pp. 362-372. D. Reidel, Holland.
van Vliet M. 1994. De invloed van de hoogte van het beeldveld op de waargenomen uurfrequentie. Radiant, Journal of the Dutch Meteor Society 16(2), 39-40.
Whipple F.L. 1951. A Comet Model. II. Physical Relations for Comets and Meteors. Astrophys. J. 113, 464-474.
Wu Z., Williams I.P. 1996. Leonid meteor storms. Mon. Not. R. Astron. Soc. 280, 1210-1218.
Yeomans D.K. 1981. Comet Tempel-Tuttle and the Leonid Meteors. Icarus 47, 492-499.
Yeomans D.K., Yau K.K., Weissman P.R. 1996. The impending appearance of comet Tempel-Tuttle and the Leonid Meteors. Icarus 124, 407-413.